Electronic Supplementary Material (ESI) for CrystEngComm.

SUPPLEMENTARY INFORMATION

Tuning photomechanical behavior and excellent elasticity of azobenzene via cocrystal engineering

Yang Ye,[a] Lei Gao,[a] Hongxun Hao,[ab] Qiuxiang Yin[ab] and Chuang Xie*[ab]

[a] School of Chemical Engineering and Technology, State Key Laboratory of Chemical Engineering, Tianjin University, Tianjin 300072, China

[b] National Collaborative Innovation Center of Chemistry Science and Engineering, Tianjin 300072, China

Table of Contents

Table S1 Crystal structure parameters of AAB, AAB-AMP and AAB-PYP. S3

Table S2 Crystal structure parameters of AAB-BIP, AAB-BPE and AAB-NPE. S4

Fig. S1 Comparison of the P-XRD patterns of experimental cocrystals and simulated results from single crystal structures. (a) AAB-AMP, (b) AAB-PYP, (c) AAB-BIP, (d) AAB-BPE, (e) AAB-NPE. S5

Fig. S2 UV-Vis DRS patterns before (blue) and after (yellow) UV irradiation (365 nm, 60 mW·cm-1, 5 min). S6

Fig. S3 Distance of the adjoining olefin C=C double bonds in AAB-NPE cocrystal. S7

Fig. S4 Microscopic observation of AAB-AMP cocrystal and its preferred orientation P-XRD pattern. S7

Fig. S5 Microscopic observation of AAB-PYP cocrystal and its preferred orientation P-XRD pattern. S8

Fig. S6 Microscopic observation of AAB-BIP cocrystal and its preferred orientation P-XRD pattern. S8

Fig. S7 Microscopic observation of AAB-BPE cocrystal and its preferred orientation P-XRD pattern. S9

Fig. S8 Scanning electron microscope picture and BFDH model of AAB-NPE cocrystal. S9

Fig. S9 (a) The dihedral angles between the plane of two different benzene rings and the dominant face (001) in AAB-BIP cocrystal. (c) The torsion angle between two benzene rings of AAB molecule in AAB-BIP cocrystal. S10

Fig. S10 Molecular stacking and N−H···N, C−H···π interactions of AAB-BIP cocrystal, N−H···N strong hydrogen bonds occupy the strongest position. S10

Fig. S11 (a) Molecule stacking of AAB-BPE cocrystal and (b) cis-trans isomer overlay of AAB molecule on dominant face (001). The width along the short axis increases by about 49.6%. (c-e) Curling behavior of AAB-BPE cocrystal along the short axis under UV irradiation, the blurred parts in (d) and (e) were formed by the curvature of the crystal away from the side of microscope lens. The moment of starting irradiation is set to 0 s, the scale bar is 200 μm. S11

Fig. S12 Strain calculation of AAB-NPE cocrystal.[2] S12

Fig. S13 The orientations of binary herringbone structures in AAB-NPE cocrystal are observed by rotating the structure along b-axis, I ~ IV and V ~ VIII are marked as blue and green, respectively. In general, it shows along the -b and +b orientations. S12

Fig. S14 (a) Crystal packing in AAB-BIP viewed down the (001), (100) and (010) faces. Binary herringbone structure can be observed from (100) face. (b) Space-filling model parallel to (001) dominant face. S13

Fig. S15 Strain calculation of AAB-BIP cocrystal.[2] S14

Supplementary movie legends S14

References S14

Table S1 Crystal structure parameters of AAB, AAB-AMP and AAB-PYP.

	AAB[1]	AAB-AMP	AAB-PYP
Formula	$C_{12}H_{11}N_3$	$C_{36}H_{38}N_{10}$	$C_{21}H_{23}N_5$
Mr	197.24	610.76	345.44
crystal color	orange	yellow	orange
crystal habit	plate	plate	plate
crystal size(mm)	-	0.2×0.18×0.16	0.2×0.18×0.12
crystal system	monoclinic	monoclinic	monoclinic
space group	$P2_1/n$	$P2_1/c$	$P2_1$
unit cell dimensions			
a [Å]	13.750(1)	7.8699(2)	7.9177(16)
b [Å]	5.6253(4)	36.0925(7)	5.9154(12)
c [Å]	14.023(1)	11.3684(3)	19.843(4)
α [°]	90	90	90
β [°]	98.400(2)	92.524(2)	90.84(3)
γ [°]	90	90	90
V [Å3]	1073.013	3226.00(13)	929.3(3)
Z	4	4	2
R-factor (%)	9.11	4.67	4.71
CCDC number	761536	2009024	2009056

Table S2 Crystal structure parameters of AAB-BIP, AAB-BPE and AAB-NPE.

	AAB-BIP	AAB-BPE	AAB-NPE
Formula	$C_{22}H_{19}N_5$	$C_{24}H_{23}N_5$	$C_{29}H_{24}N_4$
Mr	353.42	381.47	428.52
crystal color	yellow	yellow	yellow
crystal habit	plate	plate	needle
crystal size(mm)	0.16×0.14×0.12	0.2×0.16×0.14	0.2×0.18×0.12
crystal system	monoclinic	monoclinic	monoclinic
space group	$P2_1$	$P2_1$	$P2_1/n$
unit cell dimensions			
a [Å]	7.5794(4)	7.7300(6)	25.715(5)
b [Å]	5.6975(3)	5.6677(4)	5.9027(12)
c [Å]	21.4258(9)	23.0411(14)	31.344(6)
α [°]	90	90	90
β [°]	97.914(4)	91.233(6)	107.76(3)
γ [°]	90	90	90
V [$Å^3$]	916.43(8)	1009.23(12)	4531.0(17)
Z	2	2	8
R-factor (%)	5.14	7.15	7.76
CCDC number	2009026	2009027	2009057

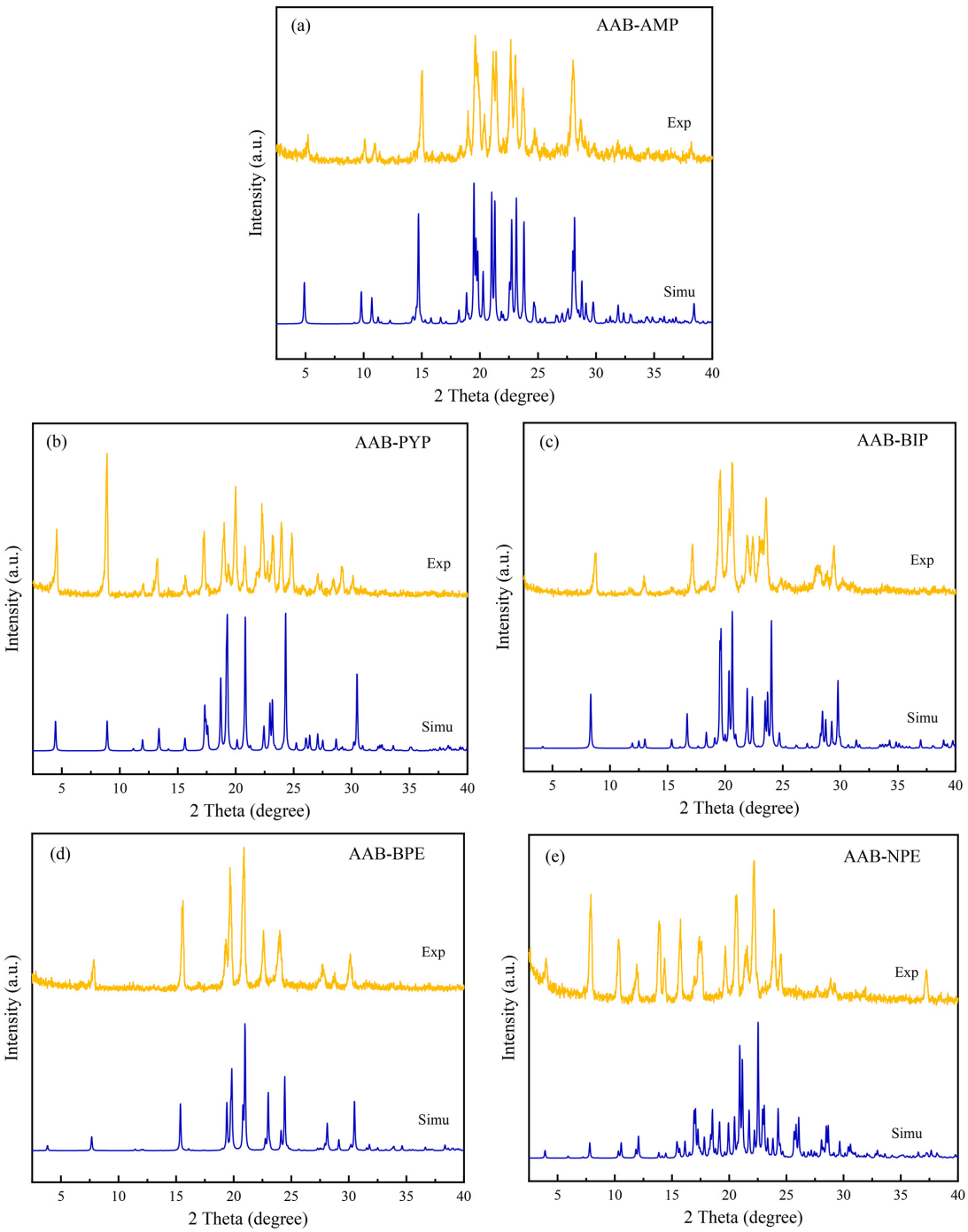

Fig. S1 Comparison of the P-XRD patterns of experimental cocrystals and simulated results from single crystal structures. (a) AAB-AMP, (b) AAB-PYP, (c) AAB-BIP, (d) AAB-BPE, (e) AAB-NPE.

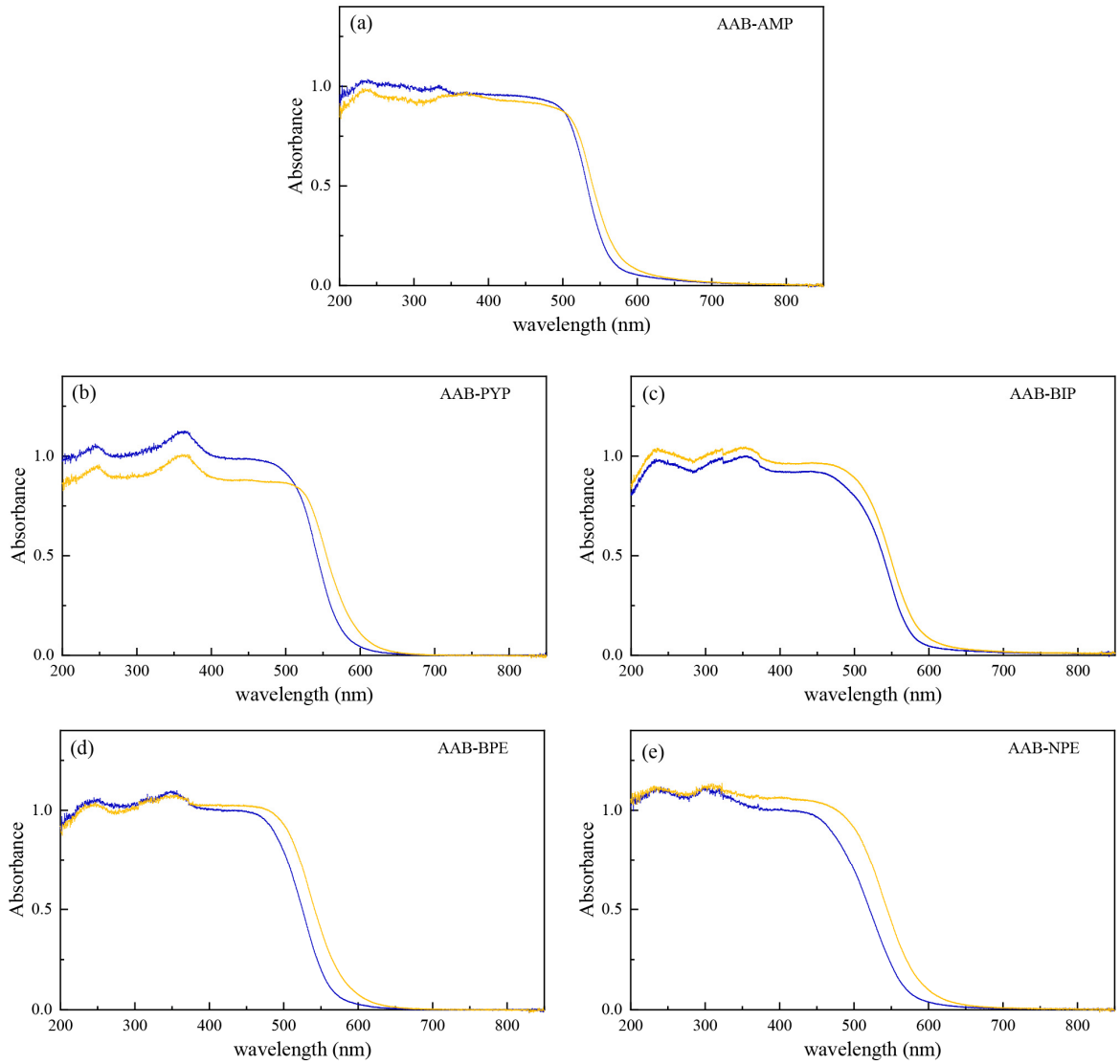

Fig. S2 UV-Vis DRS patterns before (blue) and after (yellow) UV irradiation (365 nm, 60 mW·cm-1, 5 min).

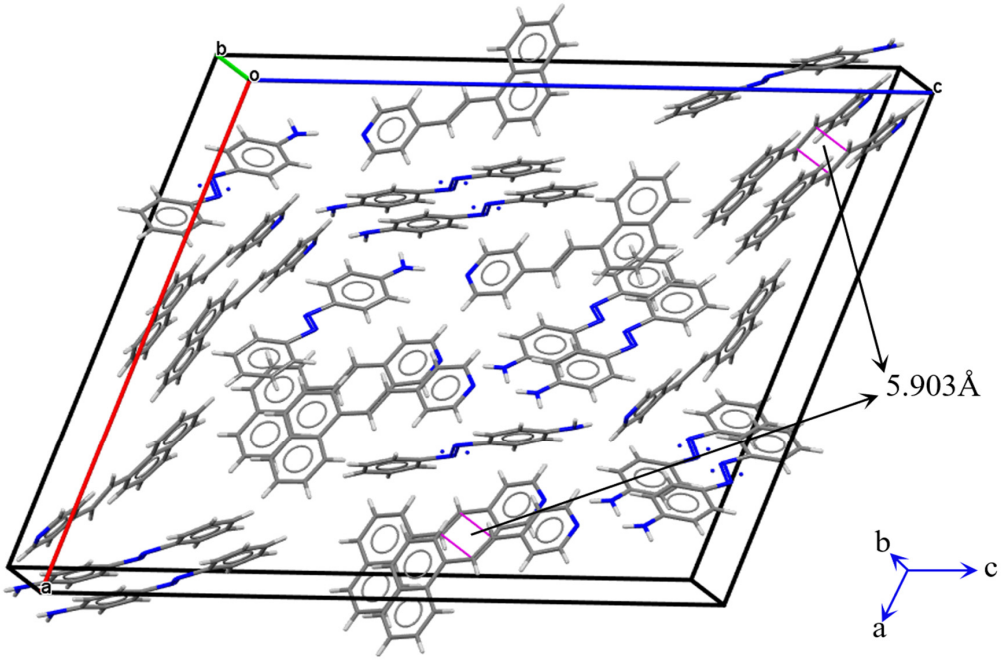

Fig. S3 Distance of the adjoining olefin C=C double bonds in AAB-NPE cocrystal.

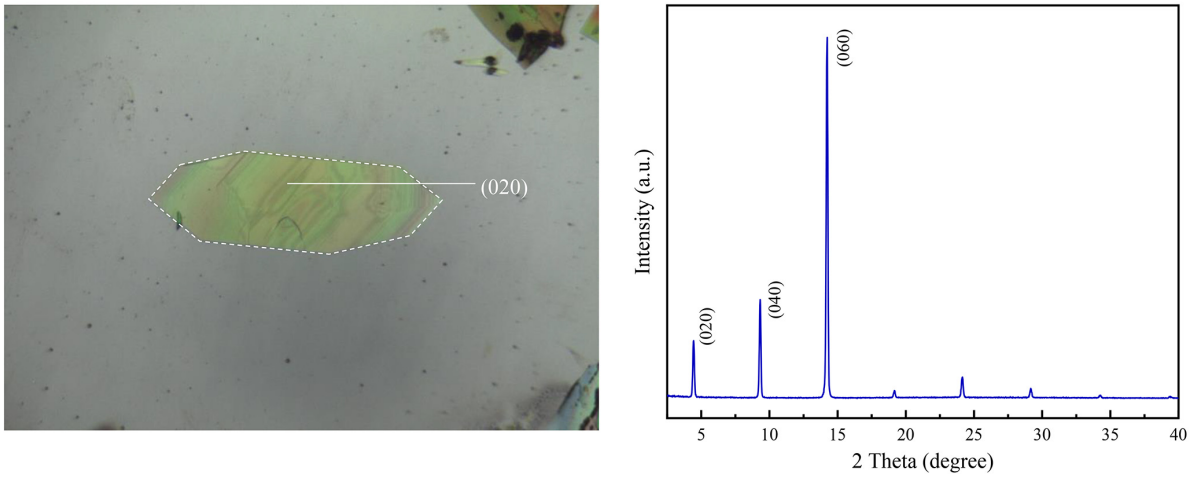

Fig. S4 Microscopic observation of AAB-AMP cocrystal and its preferred orientation P-XRD pattern.

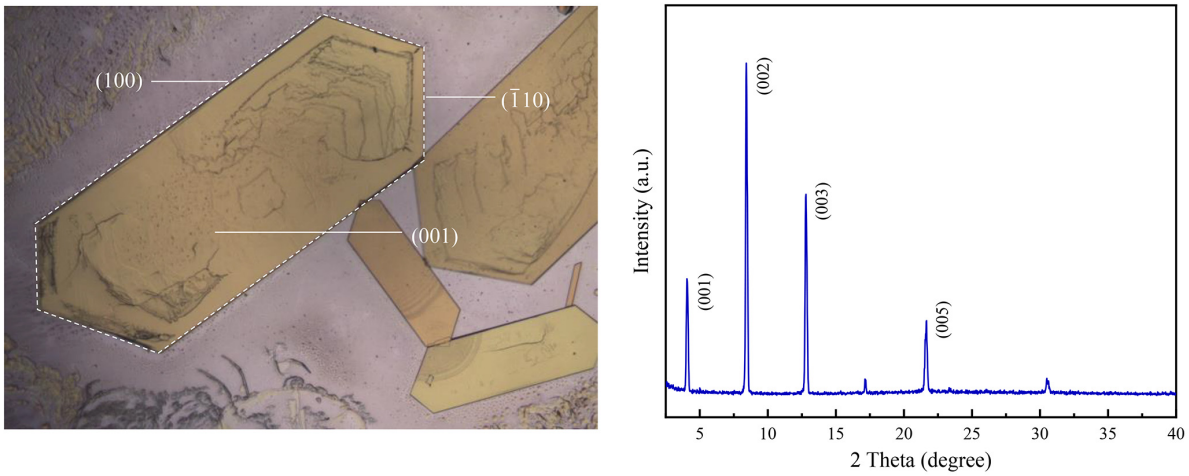

Fig. S5 Microscopic observation of AAB-PYP cocrystal and its preferred orientation P-XRD pattern.

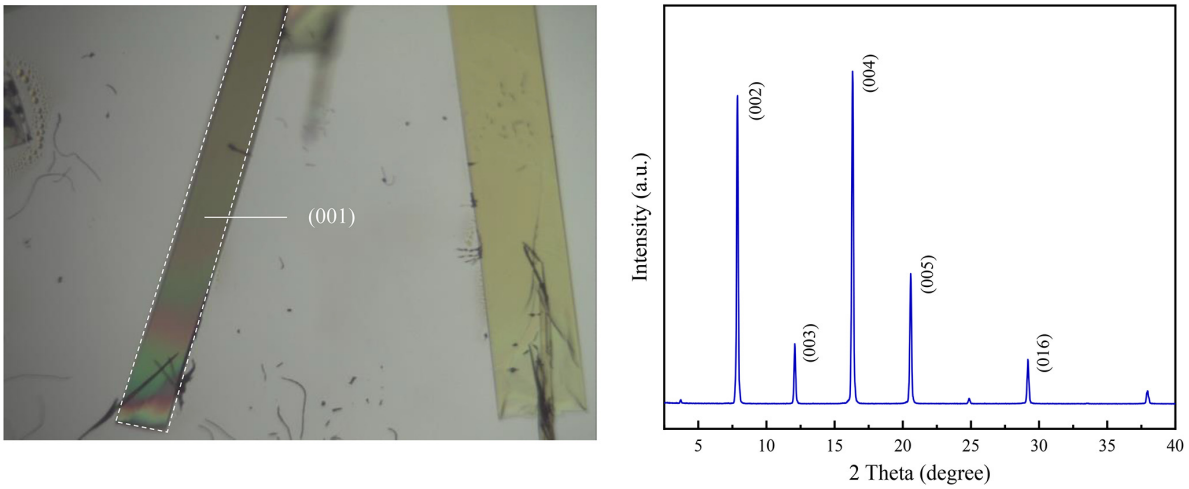

Fig. S6 Microscopic observation of AAB-BIP cocrystal and its preferred orientation P-XRD pattern.

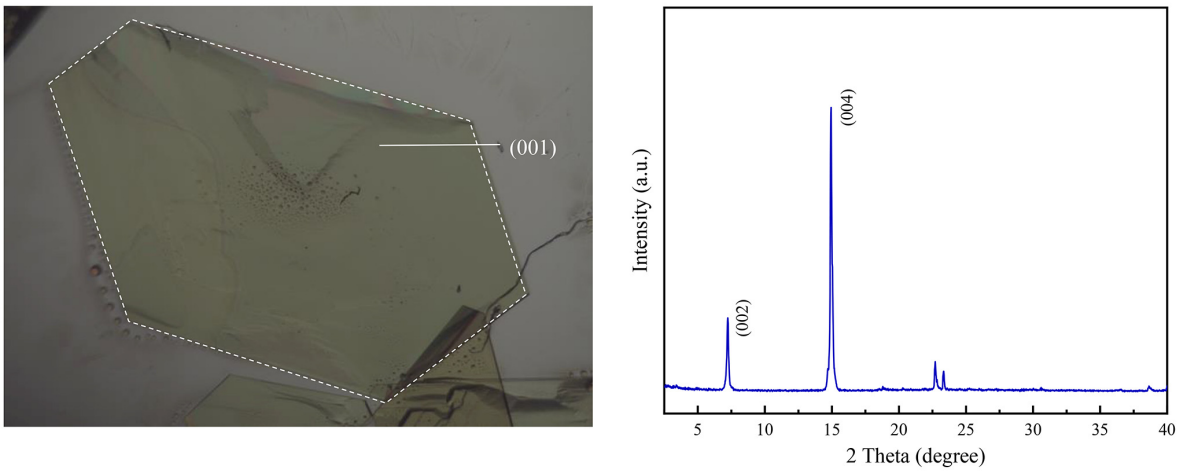

Fig. S7 Microscopic observation of AAB-BPE cocrystal and its preferred orientation P-XRD pattern.

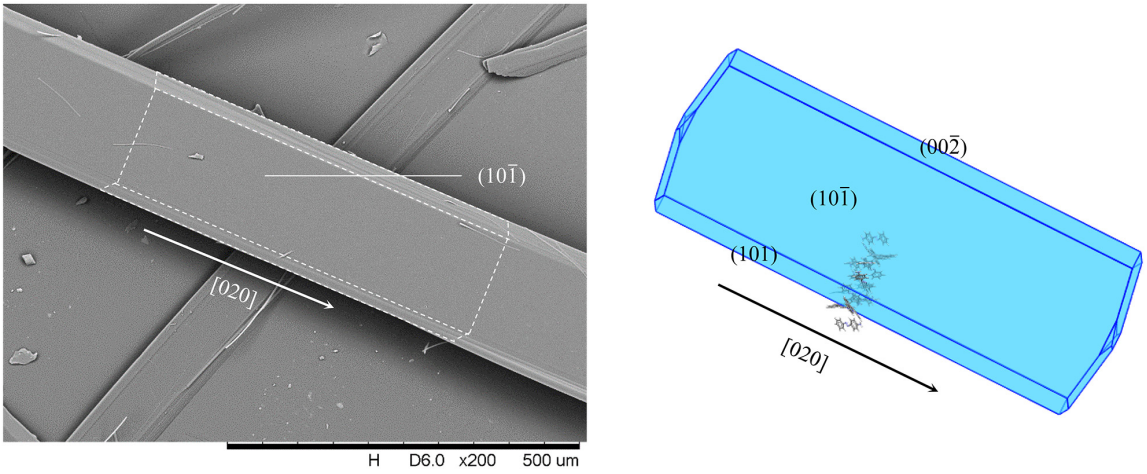

Fig. S8 Scanning electron microscope picture and BFDH model of AAB-NPE cocrystal.

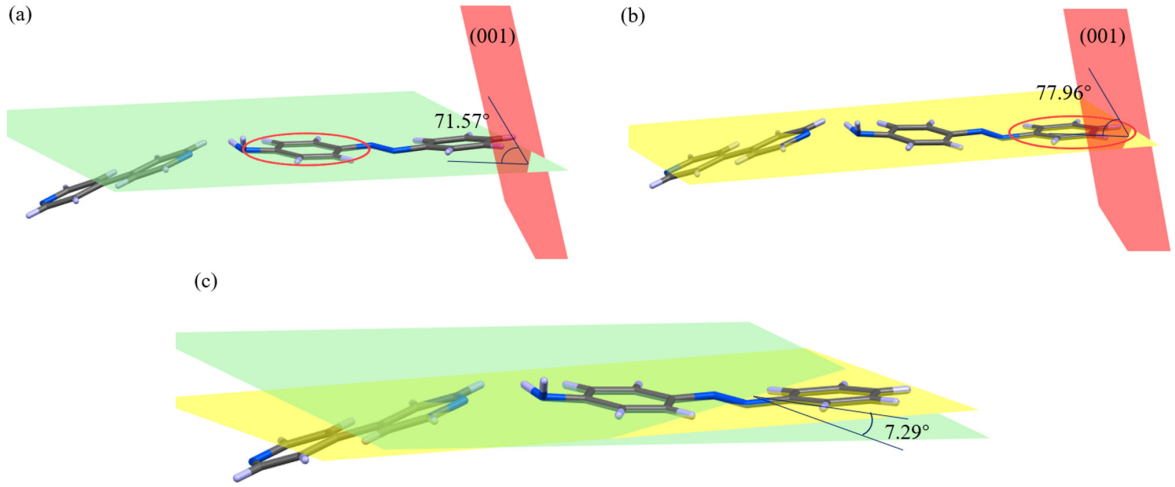

Fig. S9 (a) The dihedral angles between the plane of two different benzene rings and the dominant face (001) in AAB-BIP cocrystal. (c) The torsion angle between two benzene rings of AAB molecule in AAB-BIP cocrystal.

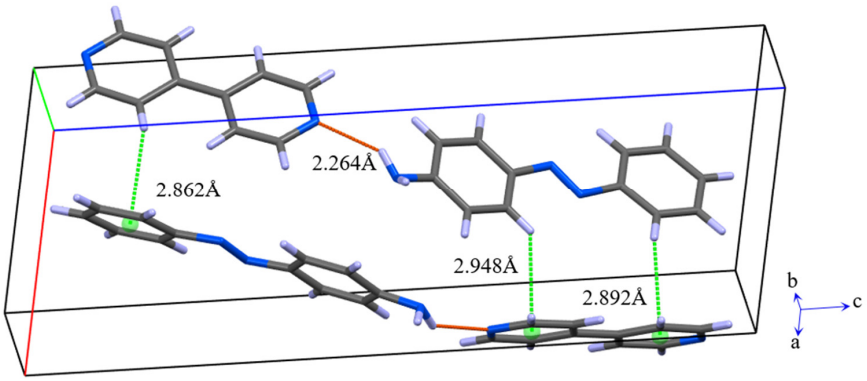

Fig. S10 Molecular stacking and N−H···N, C−H···π interactions of AAB-BIP cocrystal, N−H···N strong hydrogen bonds occupy the strongest position.

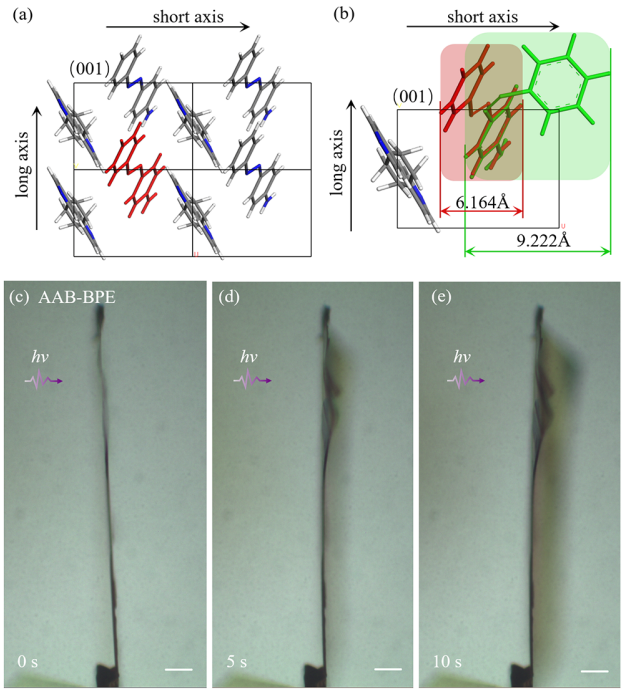

Fig. S11 (a) Molecule stacking of AAB-BPE cocrystal and (b) cis-trans isomer overlay of AAB molecule on dominant face (001). The width along the short axis increases by about 49.6%. (c-e) Curling behavior of AAB-BPE cocrystal along the short axis under UV irradiation, the blurred parts in (d) and (e) were formed by the curvature of the crystal away from the side of microscope lens. The moment of starting irradiation is set to 0 s, the scale bar is 200 μm.

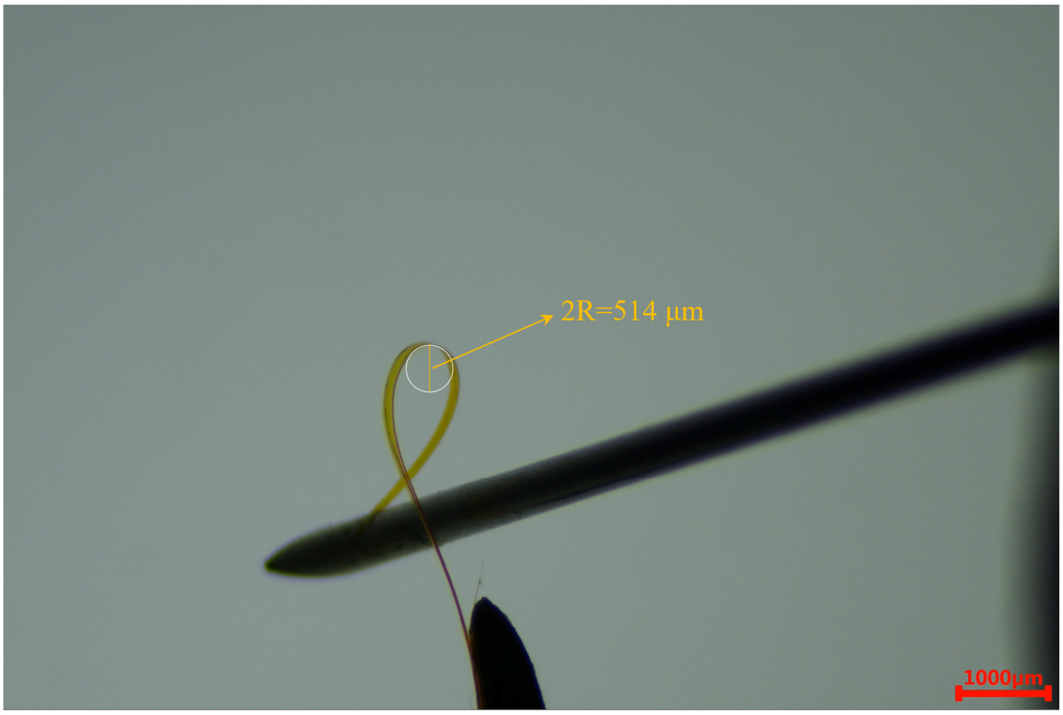

Fig. S12 Strain calculation of AAB-NPE cocrystal.[2]

$$\varepsilon=\frac{d}{2R}=\frac{16}{514}\times 100\%=3.1\%$$

d: the thickness of crystal

R: the radius of the bending curvature

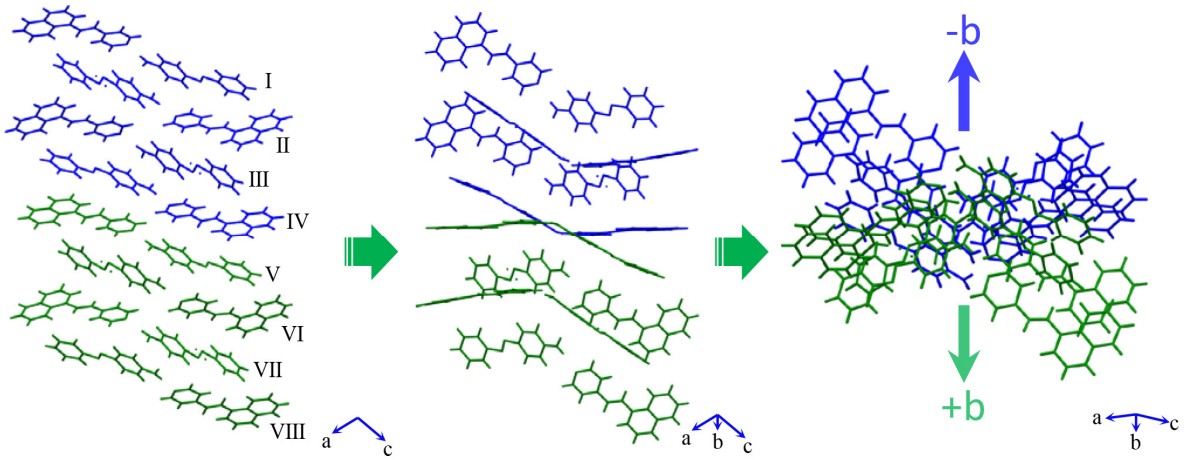

Fig. S13 The orientations of binary herringbone structures in AAB-NPE cocrystal are observed by rotating the structure along b-axis, I ~ IV and V ~ VIII are marked as blue and green, respectively. In general, it shows along the -b and +b orientations.

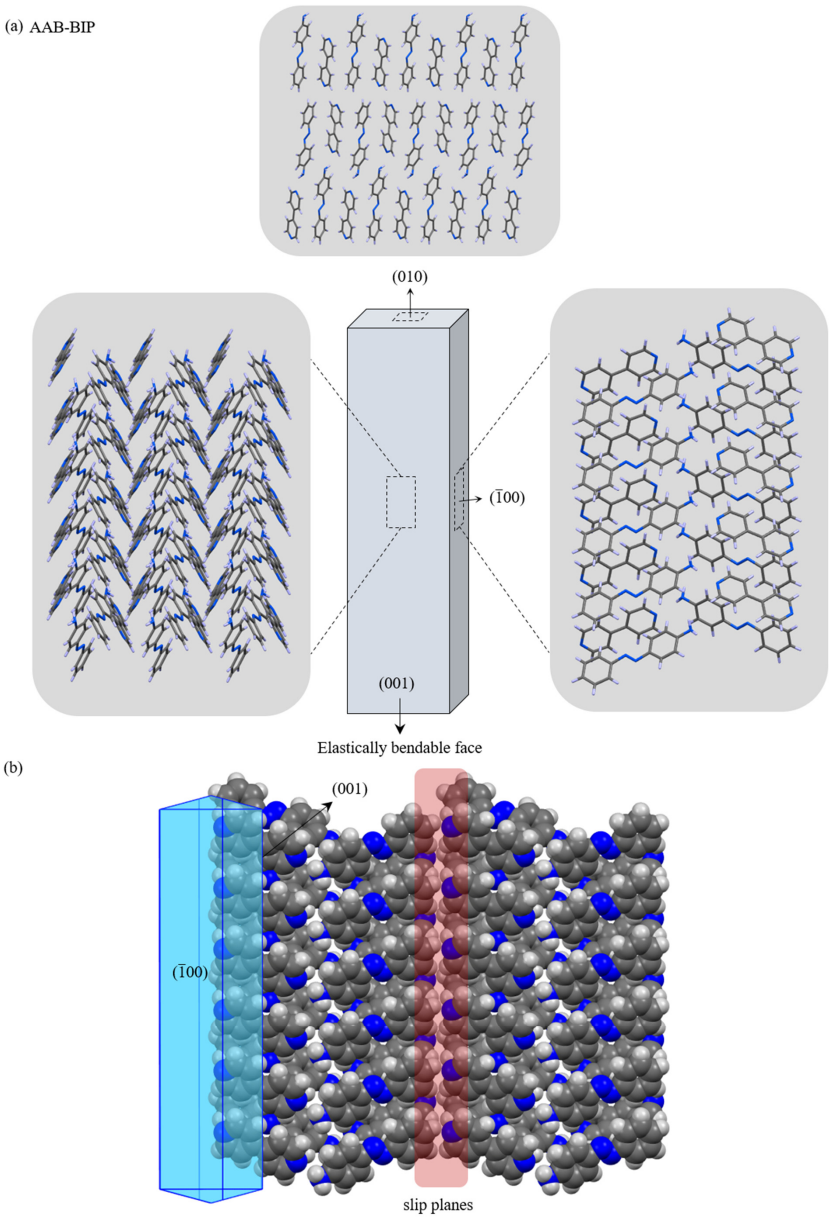

Fig. S14 (a) Crystal packing in AAB-BIP viewed down the (001), ($\bar{1}$00) and (010) faces. Binary herringbone structure can be observed from ($\bar{1}$00) face. (b) Space-filling model parallel to (001) dominant face.

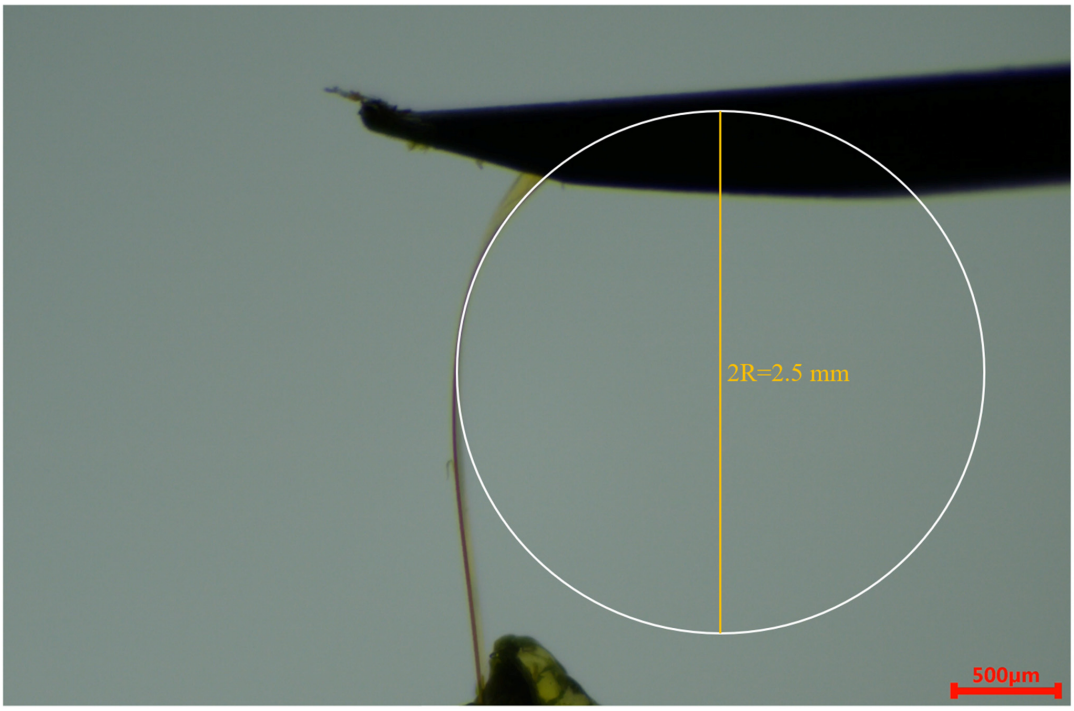

Fig. S15 Strain calculation of AAB-BIP cocrystal.[2]

$$\varepsilon=\frac{d}{2R}=\frac{0.015}{2.5}\times 100\%=0.6\%$$

d: the thickness of crystal

R: the radius of the bending curvature

Supplementary movie legends

Movie S1: Photomechanical bending process of AAB-AMP.

Movie S2: Photomechanical bending process of AAB-PYP.

Movie S3: Photomechanical bending and curling process of AAB-BIP.

Movie S4: Photomechanical bending process of AAB-BPE.

Movie S5: Photomechanical bending process of AAB-NPE.

Movie S6: Photomechanical curling process of AAB-BPE.

Movie S7: Elastic bending process of AAB-NPE.

Movie S8: Plastic bending process of AAB-BIP.

References

1. H. Nakano, *International Journal of Molecular Sciences*, 2010, **11**, 1311-1320.
2. C. Yang, J. Yoon, S. H. Kim, K. Hong, D. S. Chung, K. Heo, C. E. Park and M. Ree, *Appl. Phys. Lett.*, 2008, DOI: 10.1063/1.2948862.